XIX ANIDIS Conference, Seismic Engineering in Italy

# A note on peak inelastic displacement as a proxy for structural damage in seismic sequences

Roberto Baraschino[a,*], Georgios Baltzopoulos[a], Iunio Iervolino[a]

[a]Dipartimento di Strutture per l'Ingegneria e l'Architettura, Università degli studi di Napoli Federico II, via Claudio 21,Napoli, 80125, Italia

**Abstract**

Structural reliability assessment for a building that may experience damage accumulation during a seismic sequence can play an important role in decision making for post-earthquake repair operations or demolition and rebuilding. This typically requires the integration of the aftershock ground motion hazard at the site with the probabilistic description of the damaged building's capacity to withstand the shaking of the seismic sequence. This is usually quantified as the conditional probability that the structure, starting from a specific damage state and for given shaking intensity, will reach a more severe one. In sequence-based seismic risk studies, an analytically-derived estimate of the peak inelastic displacement is often used as a proxy for structural damage. This paper investigates the issues behind this choice and the ability of inelastic displacement demand to adequately describe structural damage due to a seismic sequence, when compared with more direct metrics of damage, such as stiffness and strength degradation. To reach this objective, a series of inelastic single-degree-of-freedom systems, having different natural period, backbones and post-elastic behavior, were subjected to sequential dynamic analysis, while considering a series of arbitrarily chosen damage states, conventionally defined by displacement demand thresholds. The investigation showed that maintaining the attractive simplicity of deformation-based damage proxies in sequence-based risk analysis, can lead to some counterintuitive representations of seismic vulnerability. Some results suggest that such problems could be alleviated if one were to consider some dependence of damage state transition thresholds on the current state of the structure.

*Keywords:* Cyclic degradation; state-dependent fragility functions;

* Corresponding author.
  *E-mail address:* roberto.baraschino2@unina.it

## 1. Introduction

Assessment of seismic reliability, according to the consolidated performance-based earthquake engineering paradigm (Cornell and Krawinkler 2000), typically assumes that earthquake damage to structures occurs in a single event of sufficient intensity to cause failure, the so-called mainshock of any seismic sequence. When this assessment is tackled with numerical tools, for example, via dynamic analysis of a structure's numerical model, there is widespread practice to use some deformation-related response measure as a proxy for structural damage, such as peak transient inelastic displacement of a control point. The extent of structural damage is often categorized into a number of discrete *damage states* (DS), each defined on the basis of exceeding a deformation threshold, and the probabilistic characterization of a structure's vulnerability to earthquakes is achieved by assigning a fragility function to each DS. These fragility functions provide the conditional probability of the structure transitioning from intact into each worse DS, in a single earthquake event of given shaking intensity. They can be analytically derived using one of several dynamic analysis strategies, such as incremental dynamic analysis (IDA; Vamvatsikos and Cornell 2002), multiple stripe analysis (Jalayer and Cornell 2009) or cloud analysis (Jalayer et al. 2015).

A seismic sequence typically contains a multitude of shaking events that occur clustered in both space and time. This implies that the structure can accumulate enough damage to lead to failure over multiple shocks, rather than in just a single event, for which there is both empirical (Iervolino et al. 2017; Sextos et al. 2018) and analytical evidence (Goda 2012; Iervolino et al. 2020; Luco et al. 2004; Ruiz-García 2012). The reliability assessment during a seismic sequence can be treated as a time-variant seismic reliability problem (Iervolino et al. 2016; Yeo and Cornell 2009). For such a treatment, structural vulnerability can be described by a set of fragility curves per DS, each enabling to obtain the conditional probability of transitioning to that DS from a less severe one, given shaking intensity. These are known as *state-dependent* fragility models and there are several proposals in the literature on how to derive them from dynamic analysis, for example using cloud analysis (Zhang et al. 2020) or *back-to-back* incremental dynamic analysis (B2B-IDA). Back-to-back IDA (e.g. Luco et al. 2004), which is the procedure adopted here, entails scaling each input ground motion until the displacement demand matches the deformation threshold corresponding to some DS and then continuing the analysis with a second accelerogram that is scaled until the structure progressively finds itself in all DS of higher severity. In this context, the transition from one damage state $DS_1$ to a more severe one $DS_2$ is often identified numerically by the exceedance of the same transient displacement threshold used for the more traditional case of transitioning from an intact state $DS_0$ to $DS_2$ (Goda 2015; Papadopoulos et al. 2020) . However, displacement demand is only an indirect measure of damage and the mechanical characteristics and/or dynamic properties of the structure at $DS_1$ may differ from their counterparts at $DS_0$. Therefore, the present study revisits this force-of-habit choice, by investigating a series of inelastic single-degree-of-freedom (SDoF) oscillators subjected to B2B-IDA. These SDoF systems are characterized by different types of *backbone* curve, that is force-displacement response to monotonic loading, and different evolutionary hysteretic laws. In all cases, dynamic analyses leading to a nominal DS threshold are followed by calculation of the damaged structures' backbones and a series of damage-related response measures are recorded on a record-by-record basis, such as residual displacement and loss of strength and/or stiffness. Fragility functions for arbitrarily defined damage states are also derived to aid in comparing the nominal vulnerability of each damaged structure with that of its intact counterpart. The results show that adopting the same displacement thresholds for the onset of a damage state, independently of whether or not the structure has already accumulated damage, can lead to a counter-intuitive situation where inelastic systems that have experienced strength and stiffness deterioration from earthquake shaking, exhibit similar seismic vulnerability as they did in their pristine state. However, the exploration of more damage-related response parameters suggests that this result may be due to limitations of peak transient drift in accounting for the effects of damage accumulation. In fact, some preliminary analyses show that if the threshold inelastic excursions were readjusted according to the initial damage state considered, some of the apparent discrepancies in state-dependent vulnerability could be alleviated.

This paper is organized in such a manner that a presentation of the adopted methodology is given first, along with a description of the case-study inelastic oscillators. Subsequently, the analysis results are presented, and state-dependent fragility functions are derived under different assumptions and compared. The paper closes with some discussion of the results and concluding remarks.

## 2. Methodology

The present investigation uses four SDoF oscillators as simple case-study inelastic structures. These are labelled as STRUCTURE 1-4 and their monotonic backbones, or pushover curves, are shown in Fig. 1, along with the trace of the hysteretic rule adopted for each oscillator. In the figure, forces and displacements have been normalized using dimensionless $\{R, \mu\}$ coordinates, where $R = F/F_y$ is the strength ratio of the restoring over the yield force of the system, and $\mu = \delta/\delta_y$ stands for the response-to-yield displacement ratio, that is, the (kinematic) ductility. The yield force and displacement values for these SDoF systems, $F_y$ and $\delta_y$, are given in Table 1 along with their periods of natural vibration $T$ and a brief description of their corresponding hysteretic behavior.
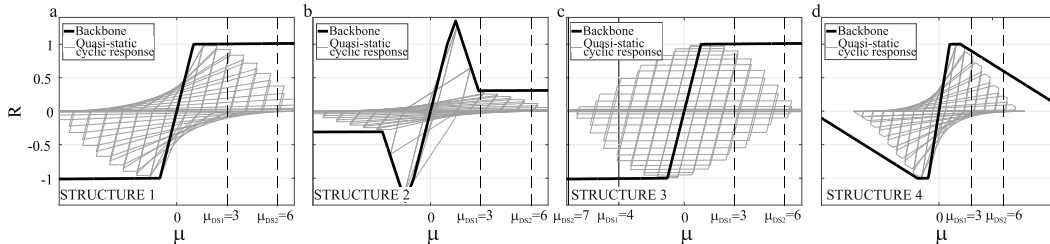


Fig. 1. Backbone curves and behaviour under quasi-static cyclic loading for the structures under investigation.

Table 1. Synopsis of the SDoF system parameters used in the investigation.

| Designation | $T$ (s) | $F_y\left(kN\right)$ | $\delta_y\left(m\right)$ | Hysteretic behavior | $\mu_{DS1}$ | $\mu_{DS2}$ |
|---|---|---|---|---|---|---|
| STRUCTURE 1 | 1.64 | 147.1 | 0.1 | peak-oriented reloading & cyclic strength degradation | 3 | 6 |
| STRUCTURE 2 | 0.78 | 480.7 | 0.1 | peak-oriented reloading & cyclic strength degradation | 3 | 6 |
| STRUCTURE 3 | 0.70 | 98.1 | 0.073 | kinematic hardening & cyclic strength degradation | 3 (4) | 6 (7) |
| STRUCTURE 4 | 0.70 | 98.1 | 0.073 | peak-oriented reloading, cyclic & in-cycle strength degradation | 4 | 11 |

STRUCTURE 1 and 2 exhibit hysteretic behavior with peak-oriented reloading stiffness, which leads to stiffness deterioration, and additionally exhibiting *cyclic* strength degradation. Note that the term cyclic degradation (FEMA 2005) is used to describe loss of strength (or stiffness) occurring in consecutive cycles in proportion to hysteretically dissipated energy, in contrast to *in-cycle* degradation that is used to describe loss of strength occurring within a single cycle when the response enters a region of negative stiffness. Under the premise that the first of these two oscillators could be considered representative of a ductile bare reinforced concrete frame, the second one could be regarded as its masonry-filled counterpart. The hysteretic behavior of STRUCTURE 3 is characterized by kinematic hardening and strength degradation, that is, a theoretical situation where loss of lateral resistance is not accompanied by loss of stiffness. Finally, STRUCTURE 4 corresponds to a peak-oriented hysteresis that is accompanied by both cyclic and in-cycle strength degradation, the latter courtesy of a softening branch starting at $\mu = 2$ and reaching zero strength, under monotonic static load, at $\mu = 12$. These yielding oscillators were modelled in the OpenSees platform (McKenna 2011), where the numerical implementation of the hysteretic behavior followed the modified Ibarra-Medina-Krawinkler model – see Ibarra et al. (2005), Lignos and Krawinkler (2011). For each oscillator, two arbitrary damage states are defined, denoted in order of severity as $DS_1$ and $DS_2$. It is initially considered that each structure transitions into these DS if the ductility demand exceeds the respective threshold values $\mu_{DS1}$ and $\mu_{DS2}$, with $\mu_{DS1} < \mu_{DS2}$; these thresholds are indicated in Fig. 1 and listed in Table 1.

All oscillators are subjected to B2B-IDA, using two sets of fifty single-component records each, with the software algorithms developed by Baltzopoulos et al. (2018). The accelerograms were taken from the NESS database (Luzi et al. 2016; Pacor et al. 2018) and the NGA-West2 database (Bozorgnia et al. 2014) and they came from events of moment magnitude ranging from 6.5 to 7.6 and Joyner-Boore distance ranging from 0 to 32 km. The two sets exhibit similar average shape and similar dispersion of spectral ordinates. Records in the first set (set 1) are always used acting on the oscillators in undamaged initial conditions, denoted here as $DS_0$. Set 1 records are scaled until maximum transient response of each system reaches the two DS thresholds $\mu_{DS1}$ and $\mu_{DS2}$. On the other hand, each record in the second set (set 2) is applied as a second shock, that is after one of the set 1 records has produced a $\mu_{DS1}$ ductility demand and the resulting oscillations have been practically damped out. The set 2 record is scaled so that a ductility

demand of $\mu_{DS2}$ is produced. In other words, the second record is, by convention, acting on an already-damaged structure in $DS_1$ and causes it to transition into $DS_2$. In this B2B-IDA, the association of a set 1 record to its sequential counterpart from set 2 is done randomly but maintained for all analyses. The polarity of both shocks is arbitrarily taken to coincide with the reported positive direction of their recording instruments. Fig. 2a shows an example response time-history during sequential application of two records as described above, with the corresponding hysteresis loops shown in panel b, plotted against the initial backbone.
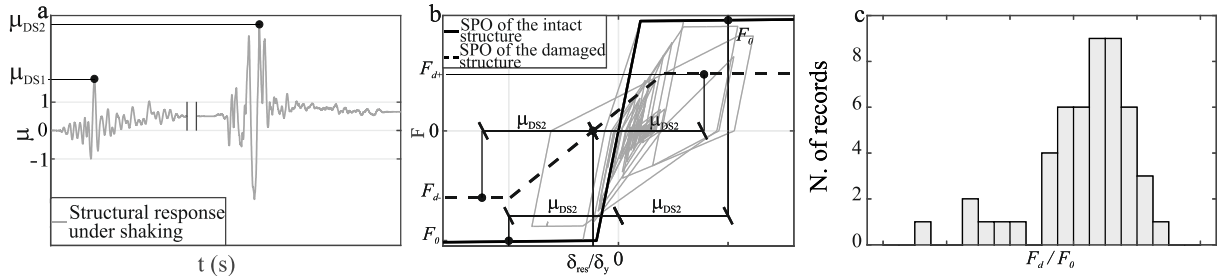


Fig. 2. (a) Response time-history, (b) initial backbone and pushover of the damaged system, (c) frequency distribution of the $F_d/F_0$ ratio.

At the end of this sequential dynamic analysis, and after the SDoF system has been left in free vibration for a duration equal to thirty times its natural period to dissipate remaining velocity, a static pushover (SPO) analysis of the damaged system is performed, with the resulting curve shown in the example of Fig. 2b as a dark dashed line. In the figure, $\delta_{res}$ is the residual displacement, while $F_0$, $F_{d+}$ and $F_{d-}$ represent the restoring force attained at ductility $\mu_{DS2}$ in the intact structure and the positive and negative loading directions of its damaged counterpart, respectively. The ratio $F_d/F_0$, where $F_d = 0.5 \cdot \left(F_{d+} + |F_{d-}|\right)$, is used to express the deteriorated lateral resistance, by virtue of representing the percentage of strength that the structure retains at $DS_2$, which can be considered as a damage measure. The third panel of the figure shows the frequency distribution of the $F_d/F_0$ ratio resulting from all fifty sequential two-record applications. As expected, although the system has nominally reached $DS_2$ in all fifty double-accelerogram sequences, as defined in terms of a deformation-based criterion, the alternative damage measure $F_d/F_0$ exhibits variability.

## 3. Results

### 3.1. Strength degradation as a damage measure

For each SDoF system considered, the procedure described in the previous section is used to calculate the ratio $F_d/F_0$ for two cases: once when the structure transitions from $DS_0$ to $DS_2$ and another for the transition from $DS_1$ to $DS_2$. According to the assumptions laid out above, the former case corresponds to records from set 1 being scaled to produce a maximum response of $\mu_{DS2}$, while the latter case corresponds to records from set 1 scaled to induce a demand of $\mu_{DS1}$, each followed by a record from set 2 scaled to result in ductility demand of $\mu_{DS2}$. The resulting frequency distributions of the ratio are shown in Fig. 3, where the location of the mean $F_d/F_0$ is indicated in each panel by a red dashed line. The upper row of panels in the figure corresponds to cases where the structure transitions from $DS_0$ to $DS_2$, with the lower row corresponding to transitions from $DS_1$ to $DS_2$.
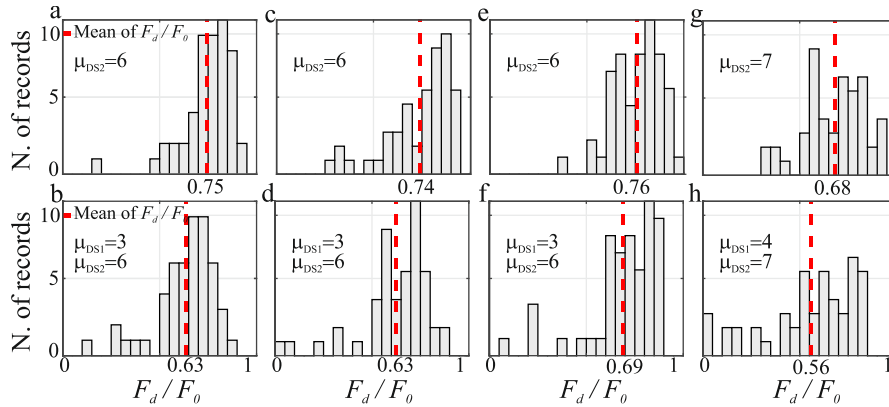
Fig. 3. Frequency distributions of the ratio $F_d/F_0$ for the investigated structures at initial state $DS_0$ (upper row) and $DS_1$ (lower row)

Panels a,b correspond to the results of STRUCTURE 1 and c,d to STRUCTURE 2. In both cases, it can be observed that the mean $F_d/F_0$ ratio for the transition from $DS_1$ to $DS_2$ is lower than the mean for the $DS_0$ to $DS_2$ case. In fact, the means between structures are almost the same, which is not surprising since $\mu_{DS1}$ corresponds to a drift where STRUCTURE 2 has lost all resistance contribution of the initial bulge of the backbone to in-cycle degradation, as can be seen in Fig. 1, and the backbone beyond that point coincides with that of the first structure by design. Panels e-h all refer to STRUCTURE 3, with the only difference that $\mu_{DS1}$ and $\mu_{DS2}$ in g,h both represent somewhat larger inelastic excursions than e,f. In all cases, the average remaining strength of the oscillators transitioning from one DS to a more severe one, is lower than that of the same system transitioning from intact conditions to the same DS, when said transitions are numerically identified via the same transient- deformation-based criterion. This difference, in terms of mean $F_d/F_0$, was about 18% for the first two cases, for which the results were similar, and 10% for the third case. That 10% difference grew to 23% for the same oscillator, when larger ductility demands were considered. The implication of this observation is that, although in all cases the same ductility demand thresholds were imposed for transition to $DS_2$, regardless of the initial state of the system, the situations where the transition started from $DS_1$, rather than $DS_0$, resulted in more average damage by comparison, at least to the extent that the ratio $F_d/F_0$ can be deemed as a possible measure of seismic damage. As a sidenote, it should be mentioned that case-study STRUCTURE 4 is hitherto conspicuously absent from the discussion of results, but only because for the $\mu_{DS2} = 11$ considered, the combination of cyclic and in-cycle degradation will practically nullify $F_d$ regardless of any other consideration.

### 3.2. Comparing state-dependent fragilities

The same B2B-IDA results are used to derive two non-parametric state-dependent fragility curves for each case, according to the procedure described in Iervolino (2017). These fragilities provide the conditional probability of exceeding $DS_2$, given some realization of a ground shaking intensity measure (IM) and an initial state, which can be either $DS_0$ (intact) or $DS_1$. The notation adopted for these models is $P\left[DS_2|DS_0,IM=im\right]$ for the former and $P\left[DS_2|DS_1,IM=im\right]$ for the latter. This operation is performed considering two different IMs, namely the spectral acceleration at the natural vibration period of each oscillator, $Sa(T)$ and an average spectral acceleration, $Sa_{avg}$, which is defined as the geometric mean of spectral ordinates at various periods – e.g., Baker and Cornell (2006). In this study, $Sa_{avg}$ is calculated considering fifty equally spaced periods within the range of 0.08s to 4s for STRUCTURE 1&2 and 0.04s to 2.8s for 3&4, in the spirit of Kohrangi et al. (2015). The resulting fragility curves are shown in Fig. 4, where panel lettering denotes direct correspondence to the cases shown in Fig. 3.
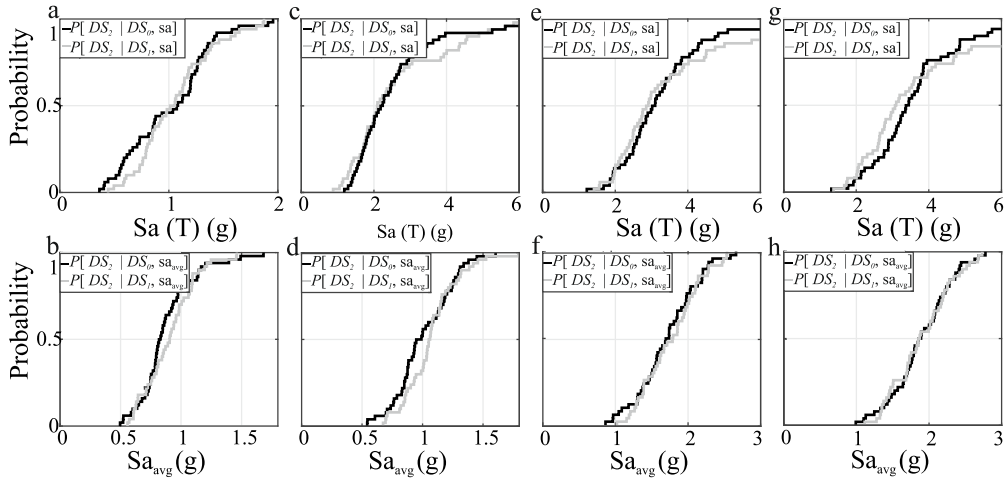
Fig. 4. State-dependent fragilities for the first three SDoF systems examined

The figure shows that in all cases, $P\left[DS_2|DS_0, IM=im\right]$ which is plotted in dark line and $P\left[DS_2|DS_1, IM=im\right]$ plotted in grey, exhibit a counter-intuitive behavior: while one would expect that the vulnerability of a structure in some DS to be larger than that of the same structure in intact conditions, which would ostensibly manifest in a shift of the grey curves to the left of the darker ones, this is not the case, with both curves remaining close to each other. This behavior has also been observed in previous studies (i.e., Goda 2015) that went ahead to caution on the ability of $Sa(T)$, as conditioning IM, to capture the expected shift in fragility. This partly motivated the inclusion of $Sa_{avg}$ as IM, which enjoys the properties of greater sufficiency and efficiency than the single spectral ordinate at large inelastic excursions (Baltzopoulos et al., 2018; Kazantzi and Vamvatsikos 2015) by virtue of reflecting spectral shape of the record over a broader period range (Bojórquez and Iervolino 2011). However, the results show that the aforementioned observation persists for both IMs. The corresponding pair of state-dependent fragilities was also derived for STRUCTURE 4, which differs from the others in that, apart from cyclic strength degradation, it also exhibits in-cycle loss of strength due to an early-setting softening branch. It should also be recalled that, in this case, $\mu_{DS1}$ is already within the negative stiffness region of the monotonic backbone, while $\mu_{DS2}$ is almost at the point of complete loss of lateral resistance, as shown in Fig. 1. In Fig. 5 the SPO curves of the SDoF system, after it has been brought to $DS_1$, are plotted against the intact monotonic backbone, one per record used to simulate the first damaging shock. The two state-dependent fragilities using both IMs are also shown.
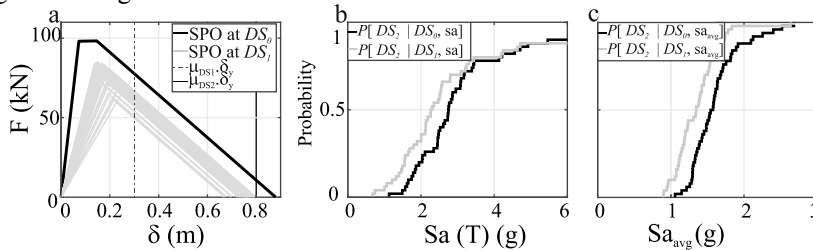


Fig. 5. For STRUCTURE 4: (a) Static pushover (SPO) of the intact and damaged system, (b-c) state-dependent fragilities

There are two observations to be made here: first, the shift of the grey $P\left[DS_2|DS_1, IM=im\right]$ curves to the left of the darker $P\left[DS_2|DS_0, IM=im\right]$ is evident for both IMs used. The second observation is that this apparent increase in vulnerability, when the system is at $DS_1$ rather than $DS_0$, is accompanied by a de facto reduction of the $\mu_{DS2}$ threshold. In fact, from the pushovers of the system when that has already nominally transitioned into $DS_1$, it is evident that the threshold that was defined on the initial backbone, is being superseded by the new points of zero lateral resistance, which have been forced to lower values than the threshold by the various degradation mechanisms.

## 3.3. Discussion

Among the investigated examples, the only case where the increase in vulnerability dictated by engineering intuition became manifest in the numerical results, was the case where the displacement threshold for the damage state was effectively modified by the nature of the hysteretic response of the oscillator. For all other cases, despite the strength and/or stiffness degradation exhibited by the hysteretic rules, the state-dependent fragilities did not appear to reflect whether the initial state was an intact or damaged system by a shift of the latter's fragility towards higher probabilities of DS transition at lower intensities. Nevertheless, the examination of another damage measure, such as the remaining ability to exert restoring force after earthquake-induced strength degradation, revealed that the oscillators that started already in $DS_1$ and then made the inelastic excursion nominally associated with $DS_2$, found themselves worse-off in terms of damage accumulation with respect to their counterparts that started from $DS_0$. Therefore, it could be argued that the counterintuitive state-dependent fragility results were a product of insisting on the numerical identification of DS transition based on the same deformation threshold regardless of the initial state. In fact, the state-dependent fragilities of the structure exhibiting in-cycle degradation were not plagued by the same issue, as the nature of the hysteretic rule adjusted the DS threshold by default, due to the contraction of the system's maximum deformation capacity. In this context, the following numerical experiment is performed: for the case of STRUCTURE 1 the $DS_2$ threshold, $\mu_{DS2}$, is arbitrarily reduced from 6 to 4.5. The justification behind this reduction is that it was found, through trial and error, that the mean $F_d/F_0$ ratio resulting from the $DS_1$ to $DS_2$ transition with this new threshold, is equal to 0.75, which is the same as that calculated for the $DS_0$ to $DS_2$ transition that is shown in Fig. 3b. The distribution of the ratio using $\mu_{DS2} = 4.5$ can be seen in Fig. 6. In other words, a reduction in the nominal inelastic excursion required to declare transition into $DS_2$, led to the same mean value of the $F_d/F_0$ damage measure that was recorded for the transition from $DS_0$ to a ductility demand of 6. Unsurprisingly, the state-dependent fragilities calculated under this new premise of a reduced transition threshold, which are also shown in Fig. 6 for both IMs considered, do reflect the aforementioned shift in vulnerability of the damaged system with respect to its intact version, all the while corresponding to an equal average loss of strength upon transition into $DS_2$.
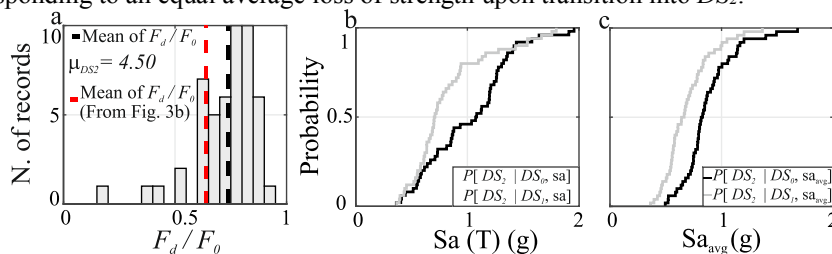


Fig. 6. For STRUCTURE 4: (a) Distribution of the loss of strength with the adjusted ductility threshold. (b)(c) State-dependent fragilities.

## 4. Final remarks

The main goal of this paper was a critical examination of the use of peak inelastic displacement as a proxy of seismic damage levels that signal a transition from a less- to a more-sever damage state. Although this is a consolidated practice when the initial state is an intact structure, its habitual extension to cases where damage accumulation passes through more damage states was put to the test, using back-to-back incremental dynamic analyses of a set of inelastic single-degree-of-freedom oscillators, whose dynamic response is characterized by different evolutionary hysteretic rules. The results showed that adopting the same ductility thresholds to identify the transition to some damage state, regardless of the initial state of the system, can lead to counterintuitive situations. In fact, there were cases where numerical analysis declared that two versions of the same structure had transitioned into the same damage state via different routes of damage accumulation, while these two versions were exhibiting different levels of quantifiable degradation. Another way of appreciating this apparent discrepancy, was through the analytical derivation of state-dependent fragility curves for arbitrarily defined damage states. In that case, there was no discernible shift in nominal seismic vulnerability between the same oscillator in intact and already-damaged state, except for one case where the type of degradation led to a reduction of deformation capacity and effectively led to a reduction of the transition threshold. Finally, it was illustrated by means of an example, though with no pretense to generality, that adopting

conventional damage state transition thresholds in terms of inelastic displacement, that somehow also account for the initial state of the system, can alleviate some of the apparent inconsistencies encountered in the preceding numerical investigations.

# References

Baker, J. W., and Cornell, C. A., 2006. Spectral Shape, Epsilon and Record Selection. Earthquake Engineering and Structural Dynamics. doi: 10.1002/eqe.571.

Baltzopoulos, G., Baraschino, R., and Iervolino, I., 2018. On the Number of Records for Structural Risk Estimation in PBEE. Earthquake Engineering & Structural Dynamics. doi: 10.1002/eqe.3145.

Baltzopoulos, G., Baraschino, R., Iervolino, I., and Vamvatsikos, D., 2018. Dynamic Analysis of Single-Degree-of-Freedom Systems (DYANAS): A Graphical User Interface for OpenSees. Engineering Structures 177(March),395–408. doi: 10.1016/j.engstruct.2018.09.078.

Bojórquez, E., and Iervolino, I., 2011. Spectral Shape Proxies and Nonlinear Structural Response. Soil Dynamics and Earthquake Engineering 31(7),996–1008. doi: 10.1016/j.soildyn.2011.03.006.

Bozorgnia, Y., Abrahamson, N. A., al Atik, L., Ancheta, T. D., Atkinson, G. M., Baker, J. W., Baltay, A., Boore, D. M., Campbell, K. W., Chiou, B. S. J., Darragh, R., Day, S., Donahue, J., Graves, R. W., Gregor, N., Hanks, T., Idriss, I. M., Kamai, R., Kishida, T., Kottke, A., Mahin, S. A., Rezaeian, S., Rowshandel, B., Seyhan, E., Shahi, S., Shantz, T., Silva, W., Spudich, P., Stewart, J. P., Watson-Lamprey, J., Wooddell, K., and Youngs, R., 2014. NGA-West2 Research Project. Earthquake Spectra 30(3),973–87. doi: 10.1193/072113EQS209M.

Cornell, C. A., and Krawinkler, H., 2000. Progress and Challenges in Seismic Performance Assessment. PEER Center News 3(2),1–3.

FEMA, 2005. FEMA-440: Improvement of Nonlinear Static Seismic Analysis Procedures. Prepared by ATC for FEMA, Washington, DC.

Goda, K., 2012. Nonlinear Response Potential of Mainshock-Aftershock Sequences from Japanese Earthquakes. Bulletin of the Seismological Society of America 102(5),2139–56. doi: 10.1785/0120110329.

Goda, K., 2015. Record Selection for Aftershock Incremental Dynamic Analysis. Earthquake Engineering and Structural Dynamics 44(7),1157–62. doi: 10.1002/eqe.2513.

Ibarra, L. F., Medina, R. A., and Krawinkler, H., 2005. Hysteretic Models That Incorporate Strength and Stiffness Deterioration. Earthquake Engineering and Structural Dynamics 34(12),1489–1511. doi: 10.1002/eqe.495.

Iervolino, I., 2017. Assessing Uncertainty in Estimation of Seismic Response for PBEE. Earthquake Engineering & Structural Dynamics 46(10),1711–23. doi: 10.1002/eqe.2883.

Iervolino, I., Baltzopoulos, G., Chioccarelli, E., and Suzuki, A., 2017. Seismic Actions on Structures in the Near-Source Region of the 2016 Central Italy Sequence. *Bulletin of Earthquake Engineering*.

Iervolino, I., Chioccarelli, E., and Suzuki, A., 2020. Seismic Damage Accumulation in Multiple Mainshock-Aftershock Sequences. Earthquake Engineering and Structural Dynamics.

Jalayer, F., and Cornell, C. A., 2009. Alternative Non-Linear Demand Estimation Methods for Probability-Based Seismic Assessments. Earthquake Engineering and Structural Dynamics 38(8),951–72. doi: 10.1002/eqe.876.

Jalayer, F., De Risi, R., and Manfredi, G., 2015. Bayesian Cloud Analysis: Efficient Structural Fragility Assessment Using Linear Regression. Bulletin of Earthquake Engineering 13(4),1183–1203. doi: 10.1007/s10518-014-9692-z.

Kazantzi, A. K., and Vamvatsikos, D., 2015. Intensity Measure Selection for Vulnerability Studies of Building Classes. Earthquake Engineering and Structural Dynamics 44(15),2677–94. doi: 10.1002/eqe.2603.

Kohrangi, M., Bazzurro, P., and Eeri, M., 2015. Vector and Scalar IM s in Structural Response Estimation : Part II – Building Demand Assessment. Earthquake Spectra 32(3),1–24. doi: 10.1193/053115EQS080M.

Lignos, D. G., and Krawinkler, H., 2011. Deterioration Modeling of Steel Components in Support of Collapse Prediction of Steel Moment Frames under Earthquake Loading. Journal of Structural Engineering 137(11),1291–1302. doi: 10.1061/(ASCE)ST.1943-541X.0000376.

Luco, N., Bazzurro, P., and Cornell, C. A., 2004. Dynamic Versus Static Computation Of The Residual Capacity Of A Mainshock-Damaged Building To Withstand An Aftershock. Proceedings of the 13th World Conference on Earthquake Engineering, Vancouver, Canada (2405).

Luzi, L., Puglia, R., Russo, E., D'Amico, M., Felicetta, C., Pacor, F., Lanzano, G., Çeken, U., Clinton, J., Costa, G., Duni, L., Farzanegan, E., Gueguen, P., Ionescu, C., Kalogeras, I., Özener, H., Pesaresi, D., Sleeman, R., Strollo, A., and Zare, M., 2016. The Engineering Strong-Motion Database: A Platform to Access Pan-European Accelerometric Data. Seismological Research Letters 87(4),987–97. doi: 10.1785/0220150278.

McKenna, F., 2011. OpenSees: A Framework for Earthquake Engineering Simulation. Computing in Science and Engineering 13(4),58–66. doi: 10.1109/MCSE.2011.66.

Pacor, F., Felicetta, C., Lanzano, G., Sgobba, S., Puglia, R., D'Amico, M., Russo, E., and Baltzopoulos, G., 2018. NESS1 : A Worldwide Collection of Strong- Motion Data to Investigate Near-Source Effects. doi: 10.1785/0220180149.

Papadopoulos, A. N., Kohrangi, M., and Bazzurro, P., 2020. Mainshock-Consistent Ground Motion Record Selection for Aftershock Sequences. Earthquake Engineering and Structural Dynamics 49(8),754–71. doi: 10.1002/eqe.3263.

Ruiz-García, J., 2012. Mainshock-Aftershock Ground Motion Features and Their Influence in Building's Seismic Response. Journal of Earthquake Engineering 16(5),719–37. doi: 10.1080/13632469.2012.663154.

Sextos, A., de Risi, R., Pagliaroli, A., Foti, S., Passeri, F., Ausilio, E., Cairo, R., Capatti, M. C., Chiabrando, F., Chiaradonna, A., Dashti, S., de Silva, F., Dezi, F., Durante, M. G., Giallini, S., Lanzo, G., Sica, S., Simonelli, A. L., and Zimmaro, P., 2018. Local Site Effects and Incremental Damage of Buildings during the 2016 Central Italy Earthquake Sequence. Earthquake Spectra 34(4),1639–69. doi: 10.1193/100317EQS194M.

Vamvatsikos, D., and Cornell, C. A., 2002. Incremental Dynamic Analysis. Earthquake Engineering and Structural Dynamics 31(3),491–514. doi: 10.1002/eqe.141.

Zhang, L., Goda, K., de Luca, F., and de Risi, R., 2020. Mainshock-Aftershock State-Dependent Fragility Curves: A Case of Wood-Frame Houses in British Columbia, Canada. Earthquake Engineering and Structural Dynamics 49(9),884–903. doi: 10.1002/eqe.3269.